Semi-analytical solutions for the problem of the electric potential set in a borehole with a highly conductive casing

Aralar Erdozain, Ignacio Muga, Victor Péron, Gabriel Pinochet

SEMI-ANALYTICAL SOLUTIONS FOR THE PROBLEM OF THE ELECTRIC POTENTIAL SET IN A BOREHOLE WITH A HIGHLY CONDUCTIVE CASING

ARALAR ERDOZAIN, IGNACIO MUGA, VICTOR PÉRON, AND GABRIEL PINOCHET

ABSTRACT. Highly conductive thin casings pose a great challenge in the numerical simulation of well-logging instruments. Witty asymptotic models may replace the presence of casings by impedance transmission conditions in those numerical simulations. The accuracy of such numerical schemes can be tested against benchmark solutions computed semi-analytically in simple geometrical configurations. This paper provides a general approach to construct those benchmark solutions for three different models: one reference model that indeed considers the presence of the casing; one asymptotic model that avoids computations in the casing domain; and one asymptotic model that reduces the presence of the casing to an interface. Our technique uses a Fourier representation of the solutions, where special care has been taken in the analytical integration of singularities to avoid numerical instabilities.

CONTENTS

Date: October 11, 2021.
Key words and phrases. Semi-analytical solutions, Asymptotic models, Electric potential, Boreholes with casing.

1. INTRODUCTION

Electrical impulses are useful resources for determining the different layers forming the Earth's subsurface. Logging instruments are commonly introduced inside wells, transmitting several impulses into the layered media, while receivers record the incoming information in real time. The obtained data is used to determine the subsurface materials by identifying their resistivity. A case of special interest corresponds to scenarii whose boreholes are surrounded by steel-made casings employed to protect the wells from possible collapses. In that case, the high conductivity of the casing, along with its thinness, greatly complicates numerical simulations. A natural way to circumvent this drawback is to consider asymptotic models avoiding the problems created by the casing [5].

Numerical approaches to simulate the described phenomena commonly consist in performing finite element or finite differences discretizations [10, 12, 13, 11, 18, 19, 17, 6]. The accuracy of these approaches requires to be always verified. A standard technique to test and verify these numerical solutions is to employ analytical methods which deliver analytical or semi-analytical solutions. Such methods provide consistent solutions in idealized scenarii at a very low computational cost.

In this paper, we consider the problem of the electric potential set in a borehole shaped domain surrounded by a metallic casing. This problem involves a realistic configuration, where the conductivity in the casing takes much higher values than those in the layered formation [14, 5]. In this configuration, the casing can be seen as a thin layer of uniform thickness ε and its conductivity is proportional to the third negative power of ε. As stated above, it is interesting to avoid this casing due to the numerical difficulties it induces. In [5], asymptotic techniques are employed to derive asymptotic models composed of impedance transmission conditions, which are specially designed to replace the casing. Stability and convergence results with respect to the parameter ε have been proved for these asymptotic models in [5].

In the present work, we will first concentrate on deriving semi-analytical solutions for different models: one reference model that considers the presence of the casing; one rigorous asymptotic model derived in [5] that avoids computations in the casing domain; and one formal asymptotic model from [7] that reduces the presence of the casing to an interface. The standard method we follow consists in employing cylindrical coordinates and assuming material homogeneity in the vertical and angular variables. In addition, the source term is represented as a Dirac delta distribution. Under these conditions, we represent the solution to each model as an inverse Fourier integral in the vertical variable, together with Fourier series in the angular variable.

Several works can be found in the literature regarding the derivation of analytical or semi-analytical solutions in cylindrical domains. For example, [9] derives semi-analytical solutions for an elasto-acoustic problem set in a borehole involving solid and fluid subdomains. In the same way, [15] derives the Green's function for the Helmholtz equation set in an infinite cylinder with Robin boundary conditions. Similar results can be found in [16], where a Green's function is obtained for the Helmholtz equation in an infinite cylinder. In [2], the authors derive an analytical solution for the Poisson equation in a cylinder with homogeneous Dirichlet boundary conditions by employing the method of separation of variables.

This paper is concerned also with numerical objectives. The semi-analytic solutions that we derive in this work are validated numerically. Then, we compare the performance of these solutions for a wide range of parameters ε. Finally, we use these semi-analytic solutions to reconstruct an experiment of Kaufman [7] which shows that the second derivative of the potential

in the vertical direction is proportional to the square root of the exterior conductivity.

The document is structured as follows. In Section 2, we set up the geometry and equations involved in our different model problems. In Section 3, we explain the procedures to derive semi-analytical solutions for the different models described in previous Section 2. Next, Section 4 is devoted to explain how we perform the inverse Fourier transform, which includes the characterization of singular behaviors and the analytic treatment of them. Several computations of this section have been shifted to the Appendix A to keep the body of the document as simple as possible. Finally, Section 5 provide numerical experiments comparing the different models, followed by conclusions in Section 6. In the end, we find an Appendix B that contains the definitions of the Bessel functions we have employed for the design of semi-analytical solutions.

2. Model problems

2.1. **Geometrical considerations.** Borehole resistivity measurements use a logging instrument equipped with transmitters and various receivers. A borehole will be modeled as a cylindrical domain covered with a thin metallic shell (the casing), which in practice serves as a wall to protect the borehole from collapse. Since the dimensions of the subsurface are much larger than the logging tool, our first simplification will be to work with unbounded cylindrical configurations. The interference produced by the logging instrument itself will not be taken into account. In order to obtain analytic representations of the physical quantities of interest, we further assume that all the media inside the borehole, at the casing, and outside the borehole, are homogeneous. Thus, we will basically work with three axisymmetric subdomains in cylindrical (r, θ, z) coordinates: one for the outer elastic material outside the shell, one for the inner fluid inside the borehole, and finally one for the metallic casing itself.

Let $\varepsilon > 0$ be the thickness of the casing and let $r_0 > 0$ be the distance from the z-axis to half the thickness of the casing. Consider the inner and outer radii of the casing, respectively characterized by

$$r_{\text{int}} := r_{\text{int}}(\varepsilon) := r_0 - \frac{\varepsilon}{2} \qquad \text{and} \qquad r_{\text{ext}} := r_{\text{ext}}(\varepsilon) := r_0 + \frac{\varepsilon}{2}.$$

Denote by $\Omega^{\varepsilon}_{\text{int}}$, $\Omega^{\varepsilon}_{\text{ext}}$, and $\Omega^{\varepsilon}_{\text{lay}}$ the inner, exterior, and casing subdomains, respectively (see Figure 1a). For a given $R_0 \gg r_0$ these domains are characterized by

$$\Omega^{\varepsilon}_{\text{int}} := \left\{(r, \theta, z) \in \mathbb{R}^3 \ : \ 0 \leq r < r_{\text{int}}\right\}, \tag{1a}$$

$$\Omega^{\varepsilon}_{\text{ext}} := \left\{(r, \theta, z) \in \mathbb{R}^3 \ : \ r_{\text{ext}} < r < R_0\right\}, \tag{1b}$$

$$\Omega^{\varepsilon}_{\text{lay}} := \left\{(r, \theta, z) \in \mathbb{R}^3 \ : \ r_{\text{int}} < r < r_{\text{ext}}\right\}. \tag{1c}$$

The interface between $\Omega^{\varepsilon}_{\text{int}}$ and $\Omega^{\varepsilon}_{\text{lay}}$ will be denoted by $\Gamma^{\varepsilon}_{\text{int}}$, while the interface between $\Omega^{\varepsilon}_{\text{lay}}$ and $\Omega^{\varepsilon}_{\text{ext}}$ will be denoted by $\Gamma^{\varepsilon}_{\text{ext}}$.

Some asymptotic models (see, e.g. [7]) do not consider the casing domain at all (the effects of the casing have been replaced by suitable impedance transmission conditions). In that situation, the model domain only considers the following two subdomains (see Figure 1b):

$$\Omega_{\text{int}} := \left\{(r, \theta, z) \in \mathbb{R}^3 \ : \ 0 \leq r < r_0\right\}, \tag{2a}$$

$$\Omega_{\text{ext}} := \left\{(r, \theta, z) \in \mathbb{R}^3 \ : \ r_0 < r < R_0\right\}, \tag{2b}$$

where the interface between Ω_{int} and Ω_{ext} is denoted by Γ.

For simplicity, we will restrict our models to the case where $R_0 = +\infty$. Otherwise, as it is customary in finite element or finite differences simulations, homogeneous boundary conditions will have to be imposed at $r = R_0$ in the forthcoming differential equations.

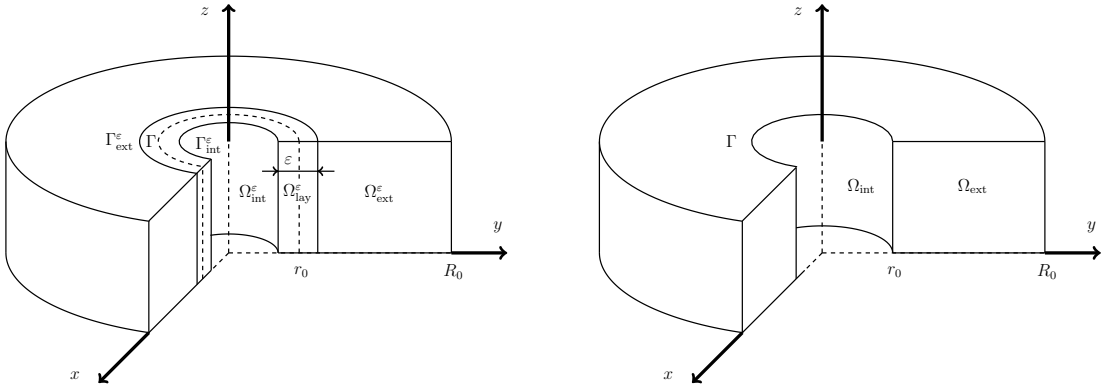

(A) With casing. (B) Without casing.

FIGURE 1. Sectioned three dimensional domains under consideration.

2.2. **Reference model.** We employ the model of the electric potential governed by the following partial differential equation:

$$\operatorname{div}(\sigma\, \nabla u) = f \quad \text{ in } \mathbb{R}^3, \tag{3}$$

where u represents the electric potential, σ stands for the conductivity of different media, and f corresponds to a current source. For our purposes, the conductivity is a piecewise constant function, with a distinct value in each homogeneous subdomain. Specifically, the value of the conductivity inside the thin layer $\Omega^\varepsilon_{\text{lay}}$ is much larger than those in the other subdomains. It has the following form (cf. [5])

$$\sigma := \sigma(\varepsilon) := \begin{cases} \sigma_{\text{int}} & \text{in } \Omega^\varepsilon_{\text{int}}, \\ \sigma_{\text{lay}} = \sigma_0 \varepsilon^{-3} & \text{in } \Omega^\varepsilon_{\text{lay}}, \\ \sigma_{\text{ext}} & \text{in } \Omega^\varepsilon_{\text{ext}}, \end{cases}$$

where $\sigma_{\text{int}},\ \sigma_0,\ \sigma_{\text{ext}} > 0$ are provided constants, and $\varepsilon > 0$ is a small parameter. We consider a point source in $(r_{\text{t}}, 0, 0) \in \Omega^\varepsilon_{\text{int}}$ given by

$$f(r, \theta, z) = \frac{A}{r} \delta(r - r_{\text{t}}) \delta(\theta) \delta(z),$$

where δ stands for the one-dimensional Dirac distribution and $A \in \mathbb{R}$ denotes an amplitude factor. Using cylindrical coordinates, eq. (3) is rewritten as

$$\Delta u = \frac{A}{\sigma_{\text{int}}\, r} \delta(r - r_{\text{t}}) \delta(\theta) \delta(z) \qquad \text{in } \Omega^\varepsilon_{\text{int}} \cup \Omega^\varepsilon_{\text{lay}} \cup \Omega^\varepsilon_{\text{ext}}, \tag{4}$$

where in cylindrical coordinates the Laplace operator becomes $\Delta(\cdot) := r^{-1}\, \partial_r(r\, \partial_r(\cdot)) + r^{-2}\, \partial^2_\theta(\cdot) + \partial^2_z(\cdot)$.

Eq. (3) impose continuity conditions on u and the normal component of $\sigma\nabla u$ across the interfaces $\Gamma^\varepsilon_{\text{int}}$ and $\Gamma^\varepsilon_{\text{ext}}$. Hence, our solution u must satisfy

$$\begin{cases} \Delta u = \dfrac{A}{\sigma_{\text{int}}\, r}\delta(r-r_{\text{t}})\delta(\theta)\delta(z) & \text{in } \Omega^\varepsilon_{\text{int}} \cup \Omega^\varepsilon_{\text{lay}} \cup \Omega^\varepsilon_{\text{ext}}, \\ [u]_{\Gamma^\varepsilon_{\text{int}}} = [u]_{\Gamma^\varepsilon_{\text{ext}}} = [\sigma\, \partial_r u]_{\Gamma^\varepsilon_{\text{int}}} = [\sigma\, \partial_r u]_{\Gamma^\varepsilon_{\text{ext}}} = 0, \end{cases} \tag{5}$$

where $[\cdot]_{\Gamma^\varepsilon_{\text{int}}}$ and $[\cdot]_{\Gamma^\varepsilon_{\text{ext}}}$ stands for the standard jump operator across the boundaries $\Gamma^\varepsilon_{\text{int}}$ and $\Gamma^\varepsilon_{\text{ext}}$, respectively. Notice that due to the use of an unbounded domain, eq. (5) must be complemented with suitable decay conditions when $r, |z| \to +\infty$.

2.3. **Asymptotic models.** The reference model of previous Subsection 2.2 can be approximated by different asymptotic models designed to replace the thin layer $\Omega^\varepsilon_{\text{lay}}$ by appropriate impedance conditions or impedance transmission conditions. First, we consider in Subsection 2.3.1 an asymptotic model which approximates the solution to the reference model (5) up to a determined order of ε. Then, we consider for comparison in Subsection 2.3.2 a formal asymptotic model developed by Kaufman [7].

2.3.1. *Fourth-order Gap-ITCs model.* In [5] it is observed that the choice of Impedance Transmission Conditions (ITCs) can lead to different asymptotics models. One of the proposed methods consists of computing the solution in the reduced domain $\Omega^\varepsilon := \mathbb{R}^3 \setminus \Omega^\varepsilon_{\text{lay}}$, thus the name Gap-ITCs. These transmission conditions are composed of jump and mean values across the interfaces, defined in the following way

$$\begin{cases} [[\,\cdot\,]]_{\Gamma^\varepsilon} & := (\cdot)_{\text{ext}}|_{\Gamma^\varepsilon_{\text{ext}}} - (\cdot)_{\text{int}}|_{\Gamma^\varepsilon_{\text{int}}}\,, \\ \{\{\,\cdot\,\}\}_{\Gamma^\varepsilon} & := \dfrac{(\cdot)_{\text{ext}}|_{\Gamma^\varepsilon_{\text{ext}}} + (\cdot)_{\text{int}}|_{\Gamma^\varepsilon_{\text{int}}}}{2}. \end{cases}$$

The fourth-order Gap-ITCs model is fully described by the following equations

$$\begin{cases} \Delta u^{[4]} & = \dfrac{A}{\sigma_{\text{int}}\, r}\delta(r-r_{\text{t}})\delta(\theta)\delta(z) & \text{in } \Omega^\varepsilon_{\text{int}} \cup \Omega^\varepsilon_{\text{ext}}, \\ [[u^{[4]}]]_{\Gamma^\varepsilon} & = 0, & \\ -\Delta_\Gamma\{\{u^{[4]}\}\}_{\Gamma^\varepsilon} & = \dfrac{\varepsilon^2}{\sigma_0}[[\sigma\, \partial_r u^{[4]}]]_{\Gamma^\varepsilon} + \dfrac{\varepsilon^3}{\sigma_0\, r_0}\{\{\sigma\, \partial_r u^{[4]}\}\}_{\Gamma^\varepsilon}, & \end{cases} \tag{6}$$

where $\Delta_\Gamma(\cdot) := r_0^{-2}\partial^2_\theta(\cdot) + \partial^2_z(\cdot)$. Under some mild conditions on the right-hand side data, it is proven in [5, Theorem 6] that the asymptotic model (6) is of order four on a bounded counterpart of Ω^ε, where homogeneous Dirichlet boundary conditions have been introduced for large values of r and z. It means that there exists a constant C independent of ε, such that for sufficiently small values of ε, the following estimate holds

$$\left\|u - u^{[4]}\right\|_{1,\Omega^\varepsilon_{\text{int}}} + \left\|u - u^{[4]}\right\|_{1,\Omega^\varepsilon_{\text{ext}}} \leq C\varepsilon^4,$$

where u is the solution to the reference problem (5) and $\|\cdot\|_{1,\mathcal{O}}$ stands for the standard Sobolev $H^1(\mathcal{O})$-norm.

2.3.2. *Interface-ITCs Kaufman model.* The other asymptotic model that we consider for comparisons, was developed in [7] by Kaufman. The method consists of computing the solution in the domains $\Omega_{\text{int}} \cup \Omega_{\text{ext}}$, ignoring the presence of the casing and replacing its influence by a suitable jump condition on the normal component of $\sigma \nabla u$, i.e.,

$$\begin{cases} \Delta u &= \dfrac{A}{\sigma_{\text{int}}\, r}\delta(r-r_{\text{t}})\delta(\theta)\delta(z), \quad \text{in } \Omega_{\text{int}} \cup \Omega_{\text{ext}}, \\ [u]_{\Gamma} &= 0, \\ [\sigma\, \partial_r u]_{\Gamma} &= -\dfrac{\sigma_0}{\varepsilon^2}\Delta_{\Gamma} u\,(r_0, z)\,, \end{cases} \tag{7}$$

where $[\,\cdot\,]_{\Gamma}$ stands for the usual jump operator at the boundary Γ. This class of models is called Interface-ITCs, since they work with an interface instead of a gap. Observe that the last condition in (7) can be thought as the last condition in (6), but removing the ε^3-term and replacing Γ^{ϵ} by Γ.

3. Derivation of semi-analytical solutions

3.1. **General solutions by means of Fourier transform.** Due to the domain invariance in the variables θ and z, the first step for deriving semi-analytical solutions consists in employing a Fourier transform along those variables, i.e.

$$\widehat{u}_k(r,\xi) = \frac{1}{2\pi}\int_{\mathbb{R}}\int_{-\pi}^{\pi} u(r,\theta,z)\cos(k\theta)\, e^{i\xi z}\,\mathrm{d}\theta\,\mathrm{d}z, \qquad k \in \mathbb{N}_0 \text{ and } \xi \in \mathbb{R}. \tag{8}$$

We emphasize that using the Fourier modes $\widehat{u}_k(r,\xi)$ we can recover the expression of u by means of the following Fourier inversion

$$u(r,\theta,z) = \sum_{k=0}^{\infty} \frac{\zeta_k}{2\pi}\int_{\mathbb{R}} \widehat{u}_k(r,\xi) e^{-i\xi z}\,\mathrm{d}\xi\cos(k\theta)\,, \quad \text{where } \zeta_k = \begin{cases} 1 \text{ if } k=0, \\ 2 \text{ if } k>0. \end{cases} \tag{9}$$

On another hand, the main equation that governs the models of this work has the form

$$\frac{1}{r}\partial_r(r\,\partial_r u) + \frac{1}{r^2}\partial_\theta^2 u + \partial_z^2 u = \frac{A}{\sigma_{\text{int}}\, r}\delta(r-r_{\text{t}})\delta(\theta)\delta(z) \quad \text{in } \Omega_*, \tag{10}$$

where Ω_* varies between the different models employed, namely

$$\Omega_* := \begin{cases} \Omega^{\varepsilon}_{\text{int}} \cup \Omega^{\varepsilon}_{\text{lay}} \cup \Omega^{\varepsilon}_{\text{ext}} & \text{for the reference model (5) (Subsection 2.2),} \\ \Omega^{\varepsilon}_{\text{int}} \cup \Omega^{\varepsilon}_{\text{ext}} & \text{for the Fourth-order Gap-ITCs model (6) (Subsection 2.3.1),} \\ \Omega_{\text{int}} \cup \Omega_{\text{ext}} & \text{for the Interface-ITCs Kaufman model (7) (Subsection 2.3.2).} \end{cases}$$

Thus, applying the Fourier transform transform (8) to equation (10) we obtain

$$\partial_r^2 \hat{u}_k + \frac{1}{r}\partial_r \hat{u}_k - \left(\frac{k^2}{r^2} + \xi^2\right)\hat{u}_k = \frac{A}{2\pi\sigma_{\text{int}} r}\delta(r-r_{\text{t}}) \qquad \text{in } I_*, \tag{11}$$

where I_* varies between the different models employed, i.e.

$$I_* := \begin{cases} (0, r_{\text{int}}) \cup (r_{\text{int}}, r_{\text{ext}}) \cup (r_{\text{ext}}, +\infty) & \text{for model (5) (Subsection 2.2),} \\ (0, r_{\text{int}}) \cup (r_{\text{ext}}, +\infty), & \text{for model (6) (Subsection 2.3.1),} \\ (0, r_0) \cup (r_0, +\infty), & \text{for model (7) (Subsection 2.3.2).} \end{cases}$$

Equation (11) defines (k, ξ)-parametrized ODEs in the r variable whose right-hand side is a one dimensional Dirac distribution. By an appropriate change of variables, we reduce these ODEs to the modified Bessel differential equation (see [1, Section 9.6]). The two linearly independent solutions in the kernel of this equation are the modified Bessel functions of the first kind $I_k(|\xi|r)$ and second kind $K_k(|\xi|r)$, see Appendix B. These functions enjoy a remarkable number of properties. We remark that I_k is bounded near zero and grows exponentially away from zero, unlike K_k which is divergent in zero and decays exponentially away from zero. Using these functions, we can build a general solution $\alpha_k(\xi, r)$ of the ODE (11) in the whole interval $(0, +\infty)$. Indeed,

$$\alpha_k(r, \xi) := \begin{cases} \dfrac{-A}{2\pi\sigma_{\text{int}}} I_k(|\xi|r)\, K_k(|\xi|r_{\text{t}}), & \text{if } r < r_{\text{t}}, \\ \dfrac{-A}{2\pi\sigma_{\text{int}}} I_k(|\xi|r_{\text{t}})\, K_k(|\xi|r), & \text{if } r_{\text{t}} < r. \end{cases} \tag{12}$$

3.2. **Reference model.** The latter implies that, for the reference model (i.e., when $I_* = (0, r_{\text{int}}) \cup (r_{\text{int}}, r_{\text{ext}}) \cup (r_{\text{ext}}, +\infty)$), we can write the solution of the eq. (11) in the following form

$$\hat{u}_k(r, \xi) = \begin{cases} c_1^k(\xi)\, I_k(|\xi|r) + \alpha_k(r, \xi) & \text{in } (0, r_{\text{int}}), \\ c_2^k(\xi)\, I_k(|\xi|r) + c_3^k(\xi)\, K_k(|\xi|r) & \text{in } (r_{\text{int}}, r_{\text{ext}}), \\ c_4^k(\xi)\, K_k(|\xi|r) & \text{in } (r_{\text{ext}}, +\infty), \end{cases} \tag{13}$$

where $c_1^k,\ c_2^k,\ c_3^k,\ c_4^k$ are coefficient functions to be determined. These four unknown functions can be computed using four equations given by the Fourier transform of the jump conditions in equation (5), i.e.,

$$[\hat{u}_k]_{\Gamma^\varepsilon_{\text{int}}} = [\hat{u}_k]_{\Gamma^\varepsilon_{\text{ext}}} = [\sigma\, \partial_r \hat{u}_k]_{\Gamma^\varepsilon_{\text{int}}} = [\sigma\, \partial_r \hat{u}_k]_{\Gamma^\varepsilon_{\text{ext}}} = 0. \tag{14}$$

Hence, the column vector $\mathbf{c}^k_{\text{ref}} := \mathbf{c}^k_{\text{ref}}(\xi) := (c_j^k(\xi))_{j=1,2,3,4}$ is the solution of a four-by-four linear system

$$\mathbf{A}^k_{\text{ref}} \mathbf{c}^k_{\text{ref}} = \mathbf{b}^k_{\text{ref}}, \tag{15}$$

where the explicit expressions for the matrix $\mathbf{A}^k_{\text{ref}}$ and the right-hand side vector $\mathbf{b}^k_{\text{ref}}$ can be found in Appendix A.

3.3. **Asymptotic models.** We examine now the equation associated with semi-analytical models (6) and (7). Proceeding analogously as in Section 3.2, we now found that Fourier modes have

the general expression

$$\hat{u}_k(r,|\xi|) = \begin{cases} c_1^k(\xi)\, I_k(|\xi|r) + \alpha_k(|\xi|,r) & \text{in } (0,r_1), \\ \\ c_2^k(\xi)\, K_k(|\xi|r) & \text{in } (r_2,+\infty), \end{cases} \tag{16}$$

where c_1^k and c_2^k are coefficient functions to be determined. In the case of Gap-ITC model (6) we put $r_1 = r_{\text{int}}$ and $r_2 = r_{\text{ext}}$; while in the case of Interface-ITCs Kaufman model (7) we put $r_1 = r_2 = r_0$.

3.3.1. *Fourth-order Gap-ITCs model.* Applying a Fourier transform to the Gap-ITCs conditions in eq. (6), we obtain

$$\begin{cases} [[\hat{u}_k]]_{\Gamma^\varepsilon} = 0, \\ \\ \left(\xi^2 + \dfrac{k^2}{r_0^2}\right) \{\{\hat{u}_k\}\}_{\Gamma^\varepsilon} = \dfrac{\varepsilon^2}{\sigma_0}[[\sigma \partial_r \hat{u}_k]]_{\Gamma^\varepsilon} + \dfrac{\varepsilon^3}{\sigma_0 r_0}\{\{\sigma \partial_r \hat{u}_k\}\}_{\Gamma^\varepsilon}, \end{cases} \tag{17}$$

where we keep the previous notation for the jump and mean values, but with the following meaning:

$$\begin{cases} [[\hat{u}_k]]_{\Gamma^\varepsilon} := \hat{u}_k(r_{\text{ext}},\cdot) - \hat{u}_k(r_{\text{int}},\cdot), \\ \\ \{\{\hat{u}_k\}\}_{\Gamma^\varepsilon} := \dfrac{u_k(r_{\text{int}},\cdot) + \hat{u}_k(r_{\text{ext}},\cdot)}{2}. \end{cases}$$

Transmission conditions (17) completely define the coefficient functions $c_1^k(\xi)$ and $c_2^k(\xi)$ of Fourier modes (16). More explicitly, the column vector $\mathbf{c}_{\text{gap}}^k := \mathbf{c}_{\text{gap}}^k(\xi) := (c_j^k(\xi))_{j=1,2}$ is the solution of a two-by-two linear system

$$\mathbf{A}_{\text{gap}}^k \mathbf{c}_{\text{gap}}^k = \mathbf{b}_{\text{gap}}^k\,, \tag{18}$$

where the explicit definition of the two-by-two matrix $\mathbf{A}_{\text{gap}}^k$ and the right-hand side vector $\mathbf{b}_{\text{gap}}^k$ can be found in Appendix A.

3.3.2. *Interface-ITCs Kaufman model.* In [7], a low-order model is proposed, with milder transmission conditions. We remark this model is defined over the domain depicted in Figure 1b. Applying the Fourier transform (8) to equation (7), the transmission conditions for the Kaufman model in Fourier domain, are described by

$$\begin{cases} [\hat{u}_k]_\Gamma = 0, \\ \\ [\sigma\, \partial_r \hat{u}_k]_\Gamma = \dfrac{\sigma_0}{\varepsilon^2}\left(\xi^2 + \dfrac{k^2}{r_0^2}\right) \hat{u}_k\,(r_0,\xi)\,. \end{cases} \tag{19}$$

Transmission conditions (19) completely define the coefficient functions $c_1^k(\xi)$ and $c_2^k(\xi)$ of the general solution (16). More explicitly, $\mathbf{c}_{\text{kau}}^k := \mathbf{c}_{\text{kau}}^k(\xi) := (c_j^k(\xi))_{j=1,2}$ is the solution of a two-by-two linear system

$$\mathbf{A}_{\text{kau}}^k \mathbf{c}_{\text{kau}}^k = \mathbf{b}_{\text{kau}}^k\,, \tag{20}$$

where the explicit definition of the two-by-two matrix $\mathbf{A}_{\text{kau}}^k$ and the right-hand side vector $\mathbf{b}_{\text{kau}}^k$ can be found in Appendix A.

4. FOURIER INVERSION

In Section 3, we have obtained a description of the solution of problem (10) by means of the Fourier modes (8). Now, we are interested in the application of the inverse Fourier transform (9) to recover the solution of (10) through those Fourier modes. The main drawback is that the Fourier mode $\hat{u}_0$ behaves singularly at $\xi = 0$, which complicates standard numerical integration. To deal with this, we apply a classical idea from previous papers (see, for similar techniques, [9, 4, 3]), which consists in characterizing the singular part of $\hat{u}_0$ (denoted hereafter by $\hat{u}_0^{\text{sing}}$), and remove it from $\hat{u}_0$ in order to define a regular part $\hat{u}_0^{\text{reg}} := \hat{u}_0 - \hat{u}_0^{\text{sing}}$. This regular part admits standard numerical Fourier inversion techniques; while the singular part is treated using analytical Fourier inversion formulae. The global Fourier inversion is reconstructed using linearity of the integral transform in (9).

The characterization of the singular part will be made using the following limiting forms of the modified Bessel functions for small arguments (see [1]):

$$I_k(z) \sim \frac{z^k}{2^k\, k!} \qquad \text{and} \qquad K_k(z) \sim \begin{cases} -\log(z), & \text{if } k = 0 \\ \dfrac{2^{k-1}\,(k-1)!}{z^k}, & \text{if } k > 0, \end{cases} \tag{21}$$

together with the derivatives formulae $I_0'(z) = I_1(z)$ and $K_0'(z) = -K_1(z)$.

To start our analysis, let us consider the fundamental solution of (4) in the whole space $\mathbb{R}^3$:

$$E := E(r, \theta, z) := \frac{A}{4\pi\, \sigma_{\text{int}}} \frac{1}{\sqrt{z^2 + r^2 + r_{\text{t}}^2 - 2 r r_{\text{t}} \cos\theta}}.$$

The Fourier modes (8) of this fundamental solution are exactly the functions $\alpha_k(r, \xi)$ defined in (12). In particular, observe that $\alpha_0(r, \xi)$ has a log-type singularity at $\xi = 0$ (see (21)). These components $\alpha_k(r, \xi)$ will be substracted from the asymptotic analysis of the Fourier modes $\hat{u}_k$ since we already know its exact Fourier inversion.

On another hand, our goal will be to evaluate the solution of the different models in the inner fluid domain, i.e., when $r < r_{\text{int}}$. Thus, we will focus our attention on the behavior of $c_1^0(\xi) I_0(|\xi| r)$ when $\xi \to 0$, for the different models under consideration. Since $I_0(|\xi| r) \sim 1$ for small arguments (see eq. (21)), every singular behavior will rely on the limiting form for small arguments of the coefficient function $c_1^0(\xi)$ obtained from the first component of the vectors $\mathbf{c}_{\text{ref}}^0, \mathbf{c}_{\text{gap}}^0, \mathbf{c}_{\text{kau}}^0$, which correspond to the solution of linear systems (15), (18) and (20), for $k = 0$, respectively.

First, we compute the determinants $\det \mathbf{A}_{\text{ref}}^0$, $\det \mathbf{A}_{\text{gap}}^0$ and $\det \mathbf{A}_{\text{kau}}^0$. Using the limiting forms in eq. (21) for small arguments, we obtain (reminding that $\sigma_{\text{lay}} = \sigma_0 \varepsilon^{-3}$)

$$\det \mathbf{A}_{\text{ref}}^0 \sim -\frac{\sigma_{\text{lay}}}{r_{\text{int}}} \frac{\sigma_{\text{ext}}}{r_{\text{ext}}}, \qquad \det \mathbf{A}_{\text{gap}}^0 \sim -\left(\frac{\varepsilon^3}{2 r_0} + \varepsilon^2\right) \frac{1}{\sigma_0} \frac{\sigma_{\text{ext}}}{r_{\text{ext}}}, \qquad \text{and} \qquad \det \mathbf{A}_{\text{kau}}^0 \sim \frac{1}{r_0}.$$

The latter ensures that systems (15), (18) and (20) are solvable for small values of the ξ-variable. Hence, singularities will depend on the right-hand side of those systems.

Next, we use Cramer's rule to obtain an explicit description of the coefficient functions $c_1^0(\xi)$. Let us define $\mathbf{A}_{\text{ref}}^{0,(1)}$ to be the matrix $\mathbf{A}_{\text{ref}}^0$ whose first column has been replaced by the right-hand

side vector $\mathbf{b}^0_{\text{ref}}$. Combining Cramer's rule with the limiting forms (21) for small arguments, we get

$$c^0_{1,\text{ref}} = \frac{\det \mathbf{A}^{0,(1)}_{\text{ref}}}{\det \mathbf{A}^0_{\text{ref}}} \sim \frac{A}{2\pi\sigma_{\text{int}}} \left(\left(1 - \frac{\sigma_{\text{int}}}{\sigma_{\text{lay}}}\right) K_0(|\xi| r_{\text{int}}) + \left(\frac{\sigma_{\text{int}}}{\sigma_{\text{lay}}} - \frac{\sigma_{\text{int}}}{\sigma_{\text{ext}}}\right) K_0(|\xi| r_{\text{ext}}) \right). \quad (22)$$

Proceeding analogously for $\mathbf{A}^0_{\text{gap}}$ and $\mathbf{A}^0_{\text{kau}}$, we get

$$c^0_{1,\text{gap}} = \frac{\det \mathbf{A}^{0,(1)}_{\text{gap}}}{\det \mathbf{A}^0_{\text{gap}}} \sim \frac{A}{2\pi\sigma_{\text{int}}} \left(K_0(|\xi| r_{\text{int}}) + \frac{\epsilon_1}{\epsilon_2} \frac{\sigma_{\text{int}}}{\sigma_{\text{ext}}} \frac{r_{\text{ext}}}{r_{\text{int}}} K_0(|\xi| r_{\text{ext}}) \right), \quad (23)$$

$$c^0_{1,\text{kau}} = \frac{\det \mathbf{A}^{0,(1)}_{\text{kau}}}{\det \mathbf{A}^0_{\text{kau}}} \sim \frac{A}{2\pi\sigma_{\text{int}}} \left(1 - \frac{\sigma_{\text{int}}}{\sigma_{\text{ext}}}\right) K_0(|\xi| r_0), \quad (24)$$

where

$$\epsilon_1 := \frac{\varepsilon}{2r_0} - 1, \quad \text{and} \quad \epsilon_2 := \frac{\varepsilon}{2r_0} + 1.$$

With a full description of the singularities of the coefficient functions $c^1_0(\xi)$, we can write the regular parts of the Fourier modes $\hat{u}_0$, which are going to be inverted using numerical quadratures. These regular parts will be defined by

$$\begin{aligned} \hat{u}^{\text{reg}}_{0,\text{ref}}(r, |\xi|) := c^0_{1,\text{ref}}(\xi) I_0(|\xi| r) \\ - \frac{A}{2\pi\sigma_{\text{int}}} \left(\left(1 - \frac{\sigma_{\text{int}}}{\sigma_{\text{lay}}}\right) K_0(|\xi| r_{\text{int}}) + \left(\frac{\sigma_{\text{int}}}{\sigma_{\text{lay}}} - \frac{\sigma_{\text{int}}}{\sigma_{\text{ext}}}\right) K_0(|\xi| r_{\text{ext}}) \right), \end{aligned} \quad (25)$$

$$\hat{u}^{\text{reg}}_{0,\text{gap}}(r, |\xi|) := c^0_{1,\text{gap}}(\xi) I_0(|\xi| r) - \frac{A}{2\pi\sigma_{\text{int}}} \left(K_0(|\xi| r_{\text{int}}) + \frac{\epsilon_1}{\epsilon_2} \frac{\sigma_{\text{int}}}{\sigma_{\text{ext}}} \frac{r_{\text{ext}}}{r_{\text{int}}} K_0(|\xi| r_{\text{ext}}) \right), \quad (26)$$

$$\hat{u}^{\text{reg}}_{0,\text{kau}}(r, |\xi|) := c^0_{1,\text{kau}}(\xi) I_0(|\xi| r) - \frac{A}{2\pi\sigma_{\text{int}}} \left(1 - \frac{\sigma_{\text{int}}}{\sigma_{\text{ext}}}\right) K_0(|\xi| r_0). \quad (27)$$

Figure 2 depicts the difference between the regular solutions $\hat{u}^{\text{reg}}_0(r, \xi)$ and the singular counterparts $c^0_1(\xi) I_0(\xi r)$, for small values of ξ at $r = 0$. Computations have been performed in the framework of Section 5 with the following constants $A = 1$, $\sigma_{\text{int}} = 1$, $\sigma_{\text{ext}} = 10^{-5}$, $\sigma_{\text{lay}} = 10^6$, $\varepsilon = 10^{-3}$, and $\sigma_0 = 10^{-3}$.

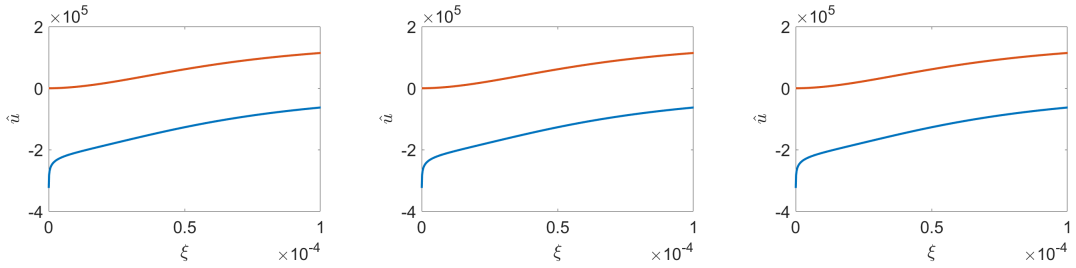

(A) Reference model (B) Gap-ITC model (C) Interface-ITC model

FIGURE 2. Extraction of the singular behavior in Fourier domain, with $\varepsilon = 0.001$. The top line is the regularized solution. The line below is the singular solution.

Finally, the singularities driven by the modified Bessel function K_0 will be treated analytically using the inversion formula (see [9, 15, 8]):

$$\frac{1}{\pi}\int_{\mathbb{R}} K_0(|\xi|r)e^{-i\xi z}\,\mathrm{d}\xi = \frac{1}{\sqrt{r^2+z^2}}.$$

5. NUMERICAL RESULTS

This Section aims to validate and compare the models presented in Section 2 and the techniques employed in Sections 3 and 4. Hereon, we employ the trapezoidal rule for numerical integration, specifically for the numerical inverse Fourier transform. We highlight that we have considered a large partition in the Fourier domain, together with refinements of this partition near zero. The refinements are required to follow smooth variations of the regular part of $\hat{u}_0$ in a neighbourhood of the origin.

We start computing the solution of the reference problem (5) for a point source centered at $(r_{\mathrm{t}}, 0, 0) = (0, 0, 0)$ and we make quantitative comparisons between this solution and the solution of the Gap-ITC model (6) proposed in [5], and the solution of the interface-ITC model (7) from [7]. For this purpose, we have considered the mid-radius of the casing placed at $r_0 = 0.165$, and different values for the thickness parameter. Namely, $\varepsilon = 0.250,\ 0.200,\ 0.150,\ 0.100,\ 0.50,$ and 0.001. We have used a normalized amplitude $A = 1$ and the following conductivities:

$$\sigma = \begin{cases} \sigma_{\mathrm{int}} = 1 & \text{in } \Omega^{\varepsilon}_{\mathrm{int}}, \\ \sigma_{\mathrm{lay}} = 10^{6} & \text{in } \Omega^{\varepsilon}_{\mathrm{lay}}, \\ \sigma_{\mathrm{ext}} = 10^{-5} & \text{in } \Omega^{\varepsilon}_{\mathrm{ext}}. \end{cases}$$

Moreover, we have considered $\sigma_0 = \sigma_{\mathrm{lay}}\varepsilon^3$ for the different values of ε. Results are depicted in Figure 3. Notice the accuracy of the fourth-order Gap-ITC solution, even for large values of the thickness parameter ε. In contrast, the larger is ε the less accurate is the solution of the interface-ITC model (7).

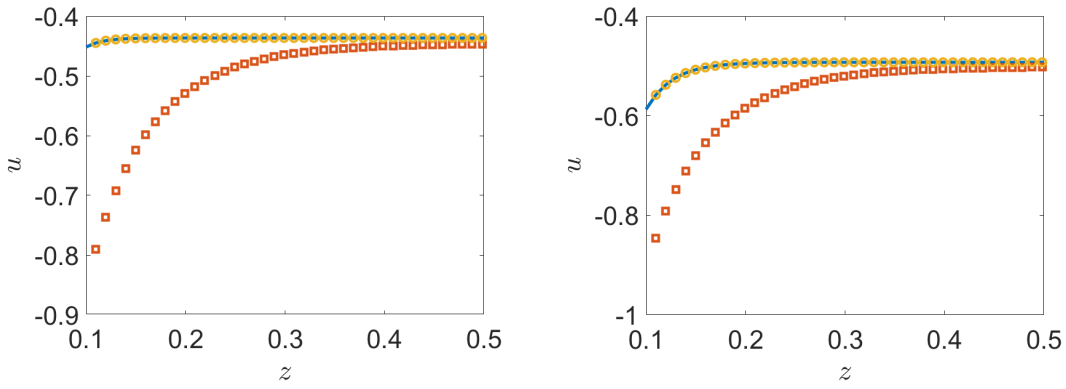

(A) $\varepsilon = 0.250$

(B) $\varepsilon = 0.200$

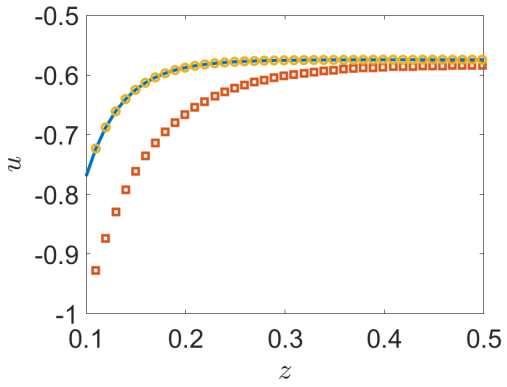

(C) $\varepsilon = 0.150$

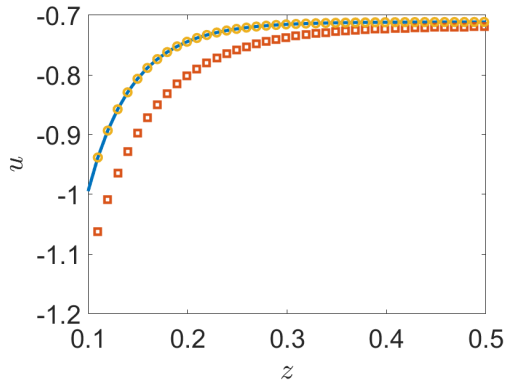

(D) $\varepsilon = 0.100$

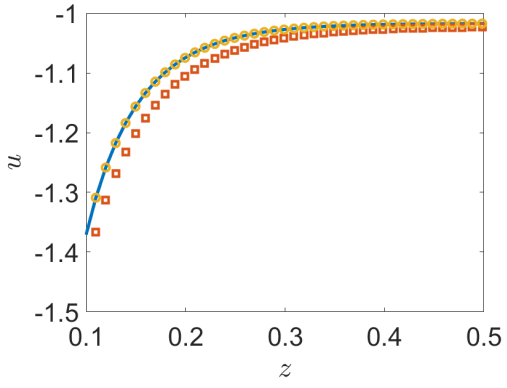

(E) $\varepsilon = 0.050$

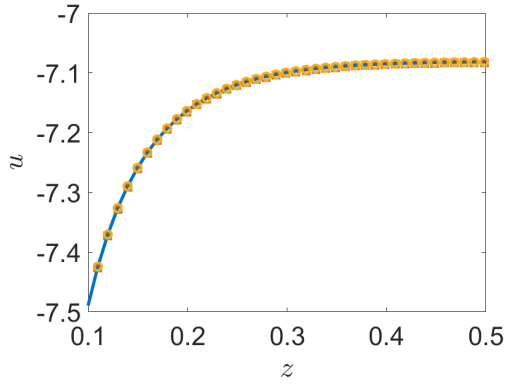

(F) $\varepsilon = 0.001$

FIGURE 3. Comparison of the different solutions in spatial domain, for different values of ε. Solid line is the reference solution. Circles for the Gap-ITC model. Squares for the Interface-ITC Kaufman model.

Next, aiming to show the versatility of the Gap-ITC model, we reconstruct one of the experiments in [7]. The objective of this experiment is to recover a relationship between the second derivative of the potential in the vertical direction and the exterior conductivity. Specifically, it is observed that the second derivative of the potential in z is proportional to the square root of the exterior conductivity, i.e. ,

$$\partial_z^2 u \approx C\,\sqrt{\sigma_{\text{ext}}}, \tag{28}$$

where $C := C(\sigma_{\text{int}})$ is independent of σ_{ext} (see [7, eq. (20) and (37)]). This proportionality is true in a certain interval of the z-axis determined by the casing thickness and the ratio $\mu := \sigma_{\text{int}}/\sigma_{\text{ext}}$. We perform computations using the Gap-ITC model (6) and the interface-ITC model (7). We have used a point source centered at $(r_{\text{t}}, 0, 0) = (0, 0, 0)$ and the mid-radius of the casing at $r_0 = 0.165$. Moreover, we have considered a fixed thickness of $\varepsilon = 0.01$, a normalized amplitude $A = 1$, and the following conductivities:

$$\sigma = \begin{cases} \sigma_{\text{int}} = 1 & \text{in } \Omega_{\text{int}}^{\varepsilon}, \\ \sigma_{\text{lay}} = 10^6 & \text{in } \Omega_{\text{lay}}^{\varepsilon}, \\ \sigma_{\text{ext}} = 1.0\text{e}-8,\ 2.0\text{e}-8,\ 1.0\text{e}-7,\ 2.0\text{e}-7,\ 2.0\text{e}-6 & \text{in } \Omega_{\text{ext}}^{\varepsilon}. \end{cases}$$

We set $\sigma_0 = \sigma_{\text{lay}}\varepsilon^3$ as before. These are the conductivities used in [7]. We discretize the z-axis using a uniform mesh of step-size $\Delta z = 0.0999$ along the interval $(1, 3000)$. Observe that in figs. 4a and 4b the solution of both model resemble each other. Moreover, in figs. 5a and 5b we obtain the expected behavior described by eq. (28), which is also corroborated in Tables 1 and 2.

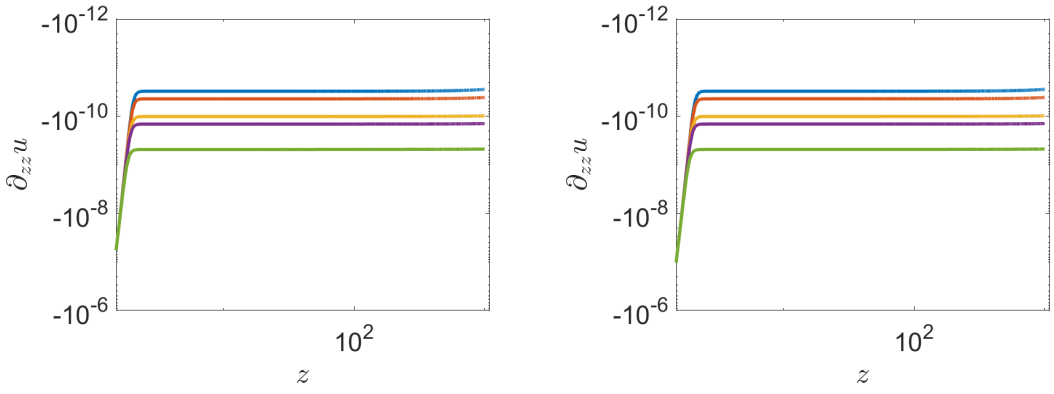

(A) Gap-ITC model (B) Interface-ITC model

FIGURE 4. $\partial_z^2 u$ for the different exterior conductivities σ_{ext}. The uppermost line corresponds to $\sigma_{\text{ext}} = 1.0\text{e}-8$; while the lowermost line corresponds to $\sigma_{\text{ext}} = 2.0\text{e}-6$.

TABLE 1. Numerical constants for $\partial_z^2 u \approx C\ \sigma_{\text{ext}}^{\alpha}$, for the Gap-ITC model, obtained with `polyfit`.

z	α	C
2.0990	0.486184337738951	15.084126468656251
20.0828	0.521227591227497	14.613303921969147
200.0207	0.521263946983287	14.615346255895707
1000.0000	0.533840363483719	14.453820826649306

TABLE 2. Numerical constants for $\partial_z^2 u \approx C\ \sigma_{\text{ext}}^{\alpha}$, for the interface-ITC model, obtained with `polyfit`.

z	α	C
2.0990	0.447393502868237	15.599943361971109
20.0828	0.521178475788366	14.615229868952285
200.0207	0.521217096294370	14.617233619952259
1000.0000	0.533814124708426	14.455410475365174

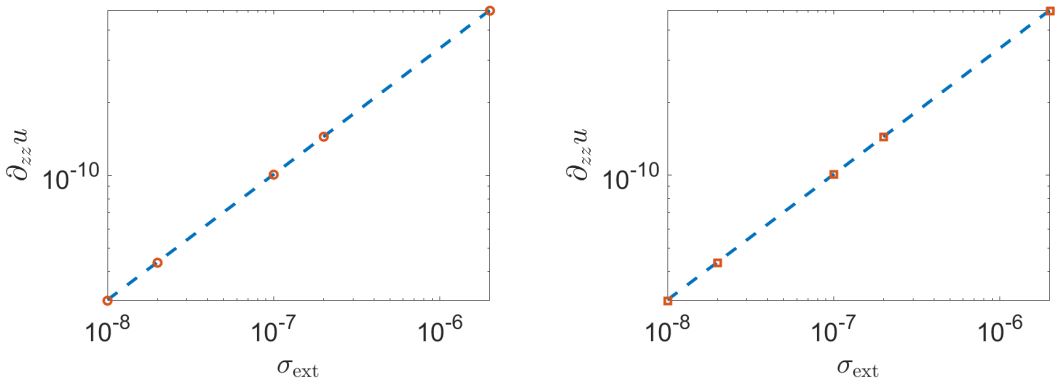

(A) Gap-ITC model (B) Interface-ITC model

FIGURE 5. Verification of eq. (28) for $z \approx 3.8974$.

6. CONCLUSIONS

We have described in detail a general framework to compute semi-analytical solutions for the electric potential problem in a borehole with highly conductive casings. This is of particular interest for testing complex numerical schemes in simple geometrical configurations. Our procedure has been applied to three different models aiming to simulate the same phenomena: one reference model that includes the casing; one asymptotic model that avoids the casing domain; and one asymptotic model that reduces the casing to an interface. Not a minor detail is the careful

extraction of singularities in Fourier domain, and the analytical treatment of their inverse Fourier transforms that we have provided. Numerical results show the robustness of the fourth-order Gap-ITC model against the interface-ITC Kaufman model for simulating the electric potential for a wide range of the thickness parameter ε. Moreover, both asymptotic models perform qualitatively equal (recovering the expected results) when used to compute the second derivative of the potential in the vertical direction for different exterior conductivities and for small values of ε.

APPENDIX A. EXPLICIT EXPRESSIONS FOR THE LINEAR SYSTEMS DEFINING THE COEFFICIENTS OF THE FOURIER MODES

As a consequence of the transmission conditions (14) over the solution (13), we observe that $\mathbf{A}^k_{\text{ref}} := \mathbf{A}^k_{\text{ref}}(\xi) := (a^k_{ij}(\xi))_{i,j=1,2,3,4}$ are defined by

$$a^k_{11}(\xi) := I_k(|\xi| r_{\text{int}}), \qquad a^k_{12}(\xi) := -I_k(|\xi| r_{\text{int}}), \qquad a^k_{13}(\xi) := -K_k(|\xi| r_{\text{int}}),$$

$$a^k_{21}(\xi) := \sigma_{\text{int}}\, I'_k(|\xi| r_{\text{int}})|\xi|, \quad a^k_{22}(\xi) := -\sigma_{\text{lay}}\, I'_k(|\xi| r_{\text{int}})|\xi|, \quad a^k_{23}(\xi) := -\sigma_{\text{lay}}\, K'_k(|\xi| r_{\text{int}})|\xi|,$$

$$a^k_{32}(\xi) := I_k(|\xi| r_{\text{ext}}), \qquad a^k_{33}(\xi) := K_k(|\xi| r_{\text{ext}}), \qquad a^k_{34}(\xi) := -K_k(|\xi| r_{\text{ext}}),$$

$$a^k_{42}(\xi) := \sigma_{\text{lay}}\, I'_k(|\xi| r_{\text{ext}})|\xi|, \quad a^k_{43}(\xi) := \sigma_{\text{lay}}\, K'_k(|\xi| r_{\text{ext}})|\xi|, \quad a^k_{44}(\xi) := -\sigma_{\text{ext}}\, K'_k(|\xi| r_{\text{ext}})|\xi|,$$

and $a^k_{14}, a^k_{24}, a^k_{31}, a^k_{41} \equiv 0$. In a similar manner, $\mathbf{b}^k_{\text{ref}} := \mathbf{b}^k_{\text{ref}}(\xi) := (b^k_i(\xi))_{i=1,2,3,4}$, are defined by

$$b^k_1(\xi) := \frac{A}{2\pi\, \sigma_{\text{int}}}\, I_k(|\xi| r_{\text{t}}) K_k(|\xi| r_{\text{int}}), \qquad b^k_2(\xi) := \frac{A}{2\pi}\, I_k(|\xi| r_{\text{t}}) K'_k(|\xi| r_{\text{int}})|\xi|,$$

and $b_3, b_4 \equiv 0$.

As a consequence of the transmission conditions (17) over the solution (16), we observe that $\mathbf{A}^k_{\text{gap}} := \mathbf{A}^k_{\text{gap}}(\xi) := (a^k_{ij}(\xi))_{i,j=1,2}$ are defined by

$$a^k_{11}(\xi) := I_k(|\xi| r_{\text{int}}),$$

$$a^k_{12}(\xi) := -K_k(|\xi| r_{\text{ext}}),$$

$$a^k_{21}(\xi) := \frac{\sigma_{\text{int}}}{\sigma_0}\left(\frac{\varepsilon^3}{2r_0} - \varepsilon^2\right) I'_k(|\xi| r_{\text{int}})\, |\xi| - \frac{1}{2}\left(\xi^2 + \frac{k^2}{r_0^2}\right) I_k(|\xi| r_{\text{int}}),$$

$$a^k_{22}(\xi) := \frac{\sigma_{\text{ext}}}{\sigma_0}\left(\frac{\varepsilon^3}{2r_0} + \varepsilon^2\right) K'_k(|\xi| r_{\text{ext}})\, |\xi| - \frac{1}{2}\left(\xi^2 + \frac{k^2}{r_0^2}\right) K_k(|\xi| r_{\text{ext}}),$$

In a similar fashion, $\mathbf{b}^k_{\text{gap}} := \mathbf{b}^k_{\text{gap}}(\xi) := (b^k_i(\xi))_{i=1,2}$, are defined by

$$b^k_1(\xi) := \frac{A}{2\pi\, \sigma_{\text{int}}}\, I_k(|\xi| r_{\text{t}}) K_k(|\xi| r_{\text{int}}),$$

$$b_2^k(\xi) := \frac{A}{2\pi\ \sigma_{\text{int}}}\ I_k(|\xi|r_{\text{t}})\left(\frac{\sigma_{\text{int}}}{\sigma_0}\left(\frac{\varepsilon^3}{2r_0}-\varepsilon^2\right)K_k'(|\xi|r_{\text{int}})\ |\xi| - \frac{1}{2}\left(\xi^2+\frac{k^2}{r_0^2}\right)K_k(|\xi|r_{\text{int}})\right).$$

Finally, as a consequence of the transmission conditions (19) over the solution (16), we observe that $\mathbf{A}_{\text{kau}}^k := \mathbf{A}_{\text{kau}}^k(\xi) := (a_{ij}^k(\xi))_{i,j=1,2}$ are defined by

$$a_{11}^k(\xi) := I_k(|\xi|r_0), \qquad a_{12}^k(\xi) := -\frac{\sigma_{\text{int}}}{\sigma_{\text{ext}}}\ K_k(|\xi|r_0),$$

$$a_{21}^k(\xi) := I_k'(|\xi|r_0)|\xi|, \qquad a_{22}^k(\xi) := -K_k'(|\xi|r_0)|\xi| + \frac{1}{\varepsilon^2}\frac{\sigma_0}{\sigma_{\text{ext}}}\left(\xi^2+\frac{k^2}{r_0^2}\right)\ K_k(|\xi|r_0),$$

and $\mathbf{b}_{\text{kau}}^k := \mathbf{b}_{\text{kau}}^k(\xi) := (b_i^k(\xi))_{i=1,2}$ are given by

$$b_1^k(\xi) := \frac{A}{2\pi\ \sigma_{\text{int}}}\ I_k(|\xi|r_{\text{t}})K_k(|\xi|r_0), \qquad b_2^k(\xi) := \frac{A}{2\pi\ \sigma_{\text{int}}}\ I_k(|\xi|r_{\text{t}})K_k'(|\xi|r_0)|\xi|.$$

APPENDIX B. BESSEL FUNCTIONS

We remind the definitions of the Bessel functions of first kind and second kind, and the modified Bessel functions.

Definition 1. *Following* [1, Section 9.1]*, for $k \in \mathbb{Z}$, the Bessel functions of first kind J_k and second kind Y_k are defined as two independent solutions to the Bessel equation*

$$x^2\frac{d^2y}{dx^2} + x\frac{\mathrm{d}y}{\mathrm{d}x} + (x^2-k^2)y = 0.$$

According to the Frobenius method, it is possible to obtain the following series expression for function J_k

$$J_k(x) = \sum_{j=0}^{\infty}\frac{(-1)^j}{j!\Gamma(j+k+1)}\left(\frac{x}{2}\right)^{2j+k},$$

where Γ represents the Gamma function. Function J_k can then be used to define Y_k:

$$Y_k(x) = \lim_{l\to k}\frac{J_l(x)\cos(l\pi) - J_{-l}(x)}{\sin(l\pi)}.$$

Definition 2. *Following* [1, Section 9.6]*, for $k \in \mathbb{Z}$, the modified Bessel functions of first kind I_k and second kind K_k are defined as two independent solutions to the modified Bessel equation*

$$x^2\frac{\mathrm{d}^2y}{\mathrm{d}x^2} + x\frac{\mathrm{d}y}{\mathrm{d}x} - (x^2+k^2)y = 0.$$

Finally, we can obtain the expressions of the modified Bessel functions I_k and K_k from the definitions of the Bessel functions given in Definition 1

$$I_k(x) = \lim_{l \to k} i^{-l} J_l(ix),$$

$$K_k(x) = \lim_{l \to k} \frac{\pi}{2} \frac{I_{-l}(x) - I_l(x)}{\sin(l\pi)}.$$

ACKNOWLEDGMENTS

This project has received funding from the European Union's Horizon 2020 research and innovation programme under the Marie Sklodowska-Curie grant agreement No 777778 (MATHROCKS). G. Pinochet has received funding from the National Agency for Research and Development (ANID), Scholarship Program, Beca de Magíster Nacional 2021 - 22210496. A. Erdozain, V. Péron and I. Muga also have received funding from the European Union's Horizon 2020 research and innovation programme under the Marie Sklodowska-Curie grant agreement No 644602 (GEAGAM). I. Muga acknowledges support from the project DI Investigación Innovadora Interdisciplinaria PUCV No 039.409/2021.

REFERENCES

[1] M. Abramowitz and I. A. Stegun. *Handbook of mathematical functions: with formulas, graphs, and mathematical tables*, volume 55. Courier Corporation, 1964.
[2] D. G. Duffy. *Green's functions with applications*. CRC Press, 2015.
[3] M. Durán, E. Godoy, and J.-C. Nédélec. Computing green's function of elasticity in a half-plane with impedance boundary condition. *Comptes Rendus Mécanique*, 334(12):725–731, 2006.
[4] M. Durán, R. Hein, and J.-C. Nédélec. Computing numerically the green's function of the half-plane helmholtz operator with impedance boundary conditions. *Numerische Mathematik*, 107(2):295–314, 2007.
[5] A. Erdozain, V. Péron, and D. Pardo. Asymptotic models for the electric potential across a highly conductive casing. *Computers & Mathematics with Applications*, 76(8):1975–2000, 2018.
[6] J. Gao, M. Smirnov, M. Smirnova, and G. Egbert. 3-D DC Resistivity Forward Modeling Using the Multi-resolution Grid. *Pure and Applied Geophysics*, 177:2803–2819, 2020.
[7] A. A. Kaufman. The electrical field in a borehole with a casing. *Geophysics*, 55(1):29–38, 1990.
[8] W. Magnus and F. Oberhettinger. *Formulas and theorems for the functions of mathematical physics*. Chelsea publishing company, 1954.
[9] I. Muga, D. Pardo, P. J. Matuszyk, and C. Torres-Verdín. Semi-analytical response of acoustic logging measurements in frequency domain. *Computers & Mathematics with Applications*, 70(4):314–329, 2015.
[10] D. Pardo, L. F. Demkowicz, C. Torres-Verdín, and C. Michler. PML enhanced with a self-adaptive goal-oriented hp-finite element method: Simulation of through-casing borehole resistivity measurements. *SIAM Journal on Scientific Computing*, 30(6):2948–2964, 2008.
[11] D. Pardo, P. J. Matuszyk, V. Puzyrev, C. Torres-Verdín, M. Jin Nam, and V. M. Calo. *Modeling of Resistivity and Acoustic Borehole Logging Measurements Using Finite Element Methods*. Elsevier Science Publishing Co. Inc., 2021.
[12] D. Pardo, C. Torres-Verdín, and L. F. Demkowicz. Simulation of multifrequency borehole resistivity measurements through metal casing using a goal-oriented hp finite-element method. *Geoscience and Remote Sensing, IEEE Transactions on*, 44(8):2125–2134, 2006.
[13] D. Pardo, C. Torres-Verdin, and M. Paszynski. Simulations of 3D DC borehole resistivity measurements with a goal-oriented hp finite-element method. Part II: through-casing resistivity instruments. *Computational Geosciences*, 12(1):83–89, 2008.

[14] D. Pardo, C. Torres-Verdín, and Z. Zhang. Sensitivity study of borehole-to-surface and crosswell electromagnetic measurements acquired with energized steel casing to water displacement in hydrocarbon-bearing layers. *Geophysics*, 73(6):F261–F268, 2008.
[15] C. Pérez-Arancibia and M. Durán. On the Green's function for the Helmholtz operator in an impedance circular cylindrical waveguide. *Journal of computational and applied mathematics*, 235(1):244–262, 2010.
[16] H. Stuwe and P. Werner. A green's function approach to wave propagation and potential flow around obstacles in infinite cylindrical channels. *Mathematical methods in the applied sciences*, 19(8):607–638, 1996.
[17] T. Wang, S. Fang, and A. G. Mezzatesta. Three-Dimensional Finite-Difference Resistivity Modeling Using an Upgridding Method. *Geoscience and Remote Sensing, IEEE Transactions on*, 38(4):1544–1550, 2000.
[18] A. H. Zemanian and B. Anderson. Modeling of borehole resistivity measurements using infinite electrical grids. *Geophysics*, 52(11):1457–1586, 1987.
[19] A. H. Zemanian and H. Keon An. Finite-difference analysis of borehole flows involving domain contractions around three-dimensional anomalies. *Applied Mathematics and Computation*, 26(1):45–75, 1988.

(A. Erdozain) UNIVERSITÉ DE PAU ET DES PAYS DE L'ADOUR, E2S UPPA, CNRS, INRIA, ÉQUIPE MAGIQUE 3D, LMAP CNRS UMR 5142, 64013 PAU, FRANCE

(I. Muga) INSTITUTO DE MATEMÁTICAS, PONTIFICIA UNIVERSIDAD CATÓLICA DE VALPARAÍSO, CASILLA 4059, VALPARAÍSO, CHILE

(V. Péron) UNIVERSITÉ DE PAU ET DES PAYS DE L'ADOUR, E2S UPPA, CNRS, INRIA, ÉQUIPE MAGIQUE 3D, LMAP CNRS UMR 5142, 64013 PAU, FRANCE

(G. Pinochet) INSTITUTO DE MATEMÁTICAS, PONTIFICIA UNIVERSIDAD CATÓLICA DE VALPARAÍSO, CASILLA 4059, VALPARAÍSO, CHILE